The Influence of Bottom Topography on the Stability of Jets in a Baroclinic Fluid

ISIDORO ORLANSKI

Geophysical Fluid Dynamics Lab., ESSA, Princeton University, Princeton, N. J.

ABSTRACT

The stability of a two-layer model is analyzed using a numerical method taking into account the effect of bottom topography. A jet in geostropic equilibrium exists in the upper layer and baroclinic instability may occur. It is found if the bottom topography has a large amplitude relative to the total depth, that it has a destabilizing rather than a stabilizing influence. Applying the model to the Gulf Stream, it is found that the most unstable disturbances, corresponding to the basic flow upstream from Cape Hatteras, are markedly different in wavelength and period from those corresponding to the basic flow downstream from Hatteras. The baroclinic disturbances in the model are consistent with the limited observational evidence on momentum transfer by Gulf Stream eddies.

1. Introduction

The purpose of this paper is to investigate the stability of a jet in a baroclinic, two-layer system and to determine the influence of bottom topography on the dynamics. Although analysis has been made of two-layer models in order to describe the dynamics of baroclinic waves in the atmosphere, there is not much known about the influence of bottom topography on such motions. There are several areas of geophysical fluid dynamics in which the above effect is relevant, e.g., the instabilities which occur in the atmosphere over the continental coast of Antartica, and the irregularities in the Kuroshio and Gulf Streams in the ocean. The extensive measurements in the Gulf Stream suggest the consideration of the latter example as a prototype in this paper. The meandering behavior of the Gulf Stream may well be explained by a stability analysis of a jet flowing over bottom topography which has a strong variation across the stream.

Early papers (Haurwitz and Panofsky, 1950; Stommel, 1953; Stern, 1961; Lipps, 1963) examined this problem by a simple stability analysis. They arrived at the conclusion that only barotropic instabilities are possible. In a later section, we will show that they arrived at this conclusion by neglecting the dynamics of one of the layers (the deep layer) and the effect of the bottom topography. We can predict this result from the necessary condition of instability for a two-layer system (Pedlosky, 1964) in which the dynamics of one of the two layers is neglected. The only possible instability in this simplified case occurs when the gradient of the mean potential vorticity of the active layer changes sign, i.e., when the horizontal shear of the jet allows

barotropic instability. We will show that the assumption of neglecting the dynamics of the lower layer and the bottom topography were not justified and that it is necessary to include both layers in the stability analysis for an adequate description of Gulf Stream behavior.

Following a formulation of the steady-state equations and the linearized perturbation equations in Sections 2 and 3, two cases are investigated in Section 4, one, Case A, being devoted to determining the eigenvalues corresponding to a cross stream variation of the bottom topography. A similarity is found between the effects of the latitudinal gradient of the Coriolis parameter and a sloping bottom topography. Under some circumstances both have a stabilizing effect on the waves, but this feature is very sensitive to the particular configuration of bottom topography considered.

In Case B the analysis will show first how the unstable mode varies when changes in the mean velocity, the wavenumber and the bottom topography are made separately. Then attention is focused on the meanders of the Gulf Stream. The large differences in bottom topography along the stream suggest the consideration of two regions (I and II). Regions I and II have representative bottom configurations similar to those in the areas upstream and downstream from Cape Hatteras, respectively. The most rapidly growing baroclinic wave has a quite different wavelength in Regions I and II.

A derivation of the energy equations and an analysis of the energetics is given in the two final sections. It is found that the mean potential energy is the source of energy for the waves, but the release of potential energy takes place in such a way that in the simple two-layer system the source of potential energy is in the deeper layer.

Oort (1964) found a countergradient heat flux in the surface layer of the Gulf Stream in Onslow Bay. Although a rigorous comparison between the two-layer model and the continuously stratified case cannot be made, the existence of an analogous source of potential energy in deeper layers of the Gulf Stream may well be possible. The solutions also indicate a small transfer of kinetic energy from the disturbances to the mean flow in complete agreement with the analysis of surface measurements in Onslow Bay made by Webster (1961a).

2. The unperturbed steady-state motion

We consider two incompressible, homogeneous fluid layers in a rotating coordinate system with constant Coriolis parameter f. The motion in each layer is hydrostatic and independent of the vertical coordinate. The two fluids are bounded above the rigid surface, $z = H_T$ and below by rigid surface, $z = h_B(x)$. The interface between the layers is at $z = h_I(x,y,t)$; $h_B \leq h_I \leq H_T$. Let $\mathbf{k}$ be a vertical unit vector; ∇ the horizontal gradient operator; $\mathbf{V}_j = (U_j, V_j)$ with $j = 1, 2$ the horizontal velocity in the upper and lower layers, respectively; and P_1 and P_2 the pressures in both layers. The equations governing the model are:

$$\left[\frac{\partial}{\partial t} + \mathbf{V}_j \cdot \nabla + f\mathbf{k} \times \right] \mathbf{V}_j = -\frac{1}{\rho_j} \nabla p_j, \qquad (2.1)$$

$$p_2 = p_1 + (\rho_2 - \rho_1) g h_I + g \rho_2 H_T, \qquad (2.2)$$

$$\left. \frac{D h_I}{Dt} \right)_1 = (H_T - h_I) \nabla \cdot \mathbf{V}_1 = W_1, \qquad (2.3)$$

$$\left. \frac{D h_I}{Dt} \right)_2 = (h_B - h_I) \nabla \cdot \mathbf{V}_2 + \mathbf{V}_2 \cdot \nabla h_B = W_2, \qquad (2.4)$$

where

$$\left. \frac{D}{Dt} \right)_j = \frac{\partial}{\partial t} + \mathbf{V}_j \cdot \nabla,$$

and W_j are the vertical velocities in both layers at the interface. The basic state consists of a velocity $\mathbf{V}_j$ in the positive y direction in each layer

$$\mathbf{V}_1 = [0, V_1(x)], \qquad (2.5)$$

$$\mathbf{V}_2 = 0, \qquad (2.6)$$

where $\mathbf{V}_1$ is only a function of x. For steady solutions of this nature, (2.1) and (2.2) require that

$$(P_2 - P_1)_x = g(\rho_2 - \rho_1) h_{Ix}, \qquad (2.7)$$

$$g(\rho_2 - \rho_1) h_{Ix} = -\rho_1 f V_1(x). \qquad (2.8)$$

Let us assume for $V_1(x)$ a jet profile of the form

$$V_1(x) = \mho x' e^{-x'}. \qquad (2.9)$$

Here $\mho$ is the amplitude of the mean velocity and x' the dimensionless coordinate $x' = x/L_s$ where L_s is a char-
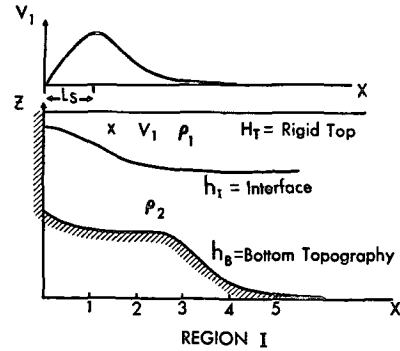

REGION I

Fig. 1. The lower part of the graph shows the two-layer model with an arbitrary bottom topography (Region I). The upper part of the diagram shows the velocity profile of the jet.

acteristic scale. Replacing (2.9) in (2.8) and integrating with respect to x, we find the interface h_I is

$$h_I = h_0 + \frac{L_s f \mho}{g'} (1 + x') e^{-x'}, \qquad (2.10)$$

where g' is the reduced gravity, $g' = (\rho_2 - \rho_1) g / \bar{\rho}$, and $\bar{\rho}$ is the average density, $\bar{\rho} = (\rho_2 + \rho_1)/2$.

Hereafter, ρ_j will be replaced by $\bar{\rho}$ in the momentum equations, an approximation frequently associated with the Boussinesq model of incompressible heterogeneous flow. We will consider two different cases for the boundaries in the x direction:

1) A semi-infinite region, $0 \leq x \leq \infty$, denoted as Region I, with a wall at $x = 0$ and an interface which does not intersect the free surface, $(H_T - h_I) > 0$ (see Fig. 1).

2) An infinite region, $-\infty \leq x \leq \infty$, denoted as Region II (see Fig. 2).

3. Perturbation equations

We allow the steady flow described in Section 1 to be perturbed by a wave-like disturbance having a small amplitude ϵ, the perturbation variables being of first and higher orders in ϵ:

$$u_j = 0 + \epsilon \, \text{Real}(\mathfrak{U}_j e^{i\psi}) + \epsilon^2 \, \text{Real} \mathfrak{U}_j'' + O(\epsilon^3), \qquad (3.1)$$

$$v_j = \bar{V}_j + \epsilon \, \text{Real}(\mathcal{V}_j e^{i\psi}) + \epsilon^2 \, \text{Real} \mathcal{V}_j'' + O(\epsilon^3), \qquad (3.2)$$
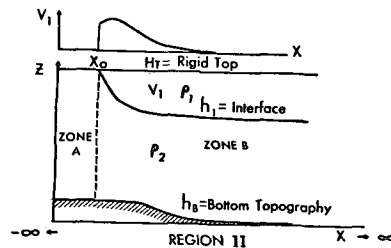

REGION II

Fig. 2. The two-layer model shown in the lower part of the figure has an interface which intersects the free surface (Region II). The upper part of the figure shows the corresponding jet profile.

$$p_j = \bar{P}_j + \epsilon \, \text{Real}(\mathcal{P}_j e^{i\psi}) + \epsilon^2 \, \text{Real}\mathcal{P}_j'' + O(\epsilon^3), \quad (3.3)$$

$$h_I = \bar{h}_I + \epsilon \, \text{Real}(\mathcal{3C} e^{i\psi}) + \epsilon^2 \, \text{Real}\mathcal{3C}'' + O(\epsilon^3), \quad (3.4)$$

$$\psi = (ky + \sigma t), \quad (3.5)$$

where $\bar{V}_j$ is the mean velocity defined in Section 2; $\bar{h}_I$ and $\bar{P}_j$ are the values defined by (2.9) and (2.2); $\mathcal{U}_j$, $\mathcal{V}_j$, $\mathcal{P}_j$ and $\mathcal{3C}$ are, in general, complex functions of x; k is the y wavenumber; and σ the frequency.

The first-order forms of (2.1)–(2.2) are:

$$\mathcal{P}_2 - \mathcal{P}_1 = g(\rho_2 - \rho_1)\mathcal{3C}, \quad (3.6)$$

$$i(\sigma + k\bar{V}_j)\mathcal{U}_j - f\mathcal{V}_j = -\mathcal{P}_{jx}/\bar{\rho}, \quad (3.7)$$

$$i(\sigma + k\bar{V}_j)\mathcal{V}_j + f\mathcal{U}_j + \mathcal{U}_j\bar{V}_{jx} = -\frac{ik\mathcal{P}_j}{\bar{\rho}}, \quad (3.8)$$

$$h_I = \bar{h}_I + \mathcal{3C}. \quad (3.9)$$

The kinematic boundary conditions at the interface are:

$$i(\sigma + k\bar{V}_1)H + U_1\bar{h}_{Ix} = (H_T - \bar{h}_I)(U_{1x} + ikV_1), \quad (3.10)$$

$$i\sigma H + U_2\bar{h}_{Ix} = (h_B - \bar{h}_I)(U_{2x} + ikV_2) + U_2h_{Bx}, \quad (3.11)$$

where $h_B(x)$ is the height of the bottom topography. The dynamic boundary condition at the interface is

$$\mathcal{P}_2 - \mathcal{P}_1 = g(\rho_2 - \rho_1)\mathcal{3C}. \quad (3.12)$$

The horizontal boundary conditions in Region I are:

$$\begin{array}{ll} x=0, & x=E_b \to \infty \\ u_1=0, \quad \mathcal{U}_1, \mathcal{V}_1 & \text{and} \quad \mathcal{P}_1 \to 0 \\ u_2=0, \quad \mathcal{U}_2, \mathcal{V}_2 & \text{and} \quad \mathcal{P}_2 \to 0 \end{array} \Bigg\}, \quad (3.13)$$

where E_b is the eastern wall.

In Region II the corresponding conditions are:

$$\begin{array}{l} x \to -\infty \leftarrow \text{Zone A} \to x=x_0 \leftarrow \text{Zone B} \to x=E_b \to \infty \\ \mathcal{P}_1 = \text{finite}, \quad \mathcal{U}_1, \mathcal{V}_1, \mathcal{P}_1 \to 0 \\ \mathcal{U}_2, \mathcal{V}_2 \text{ and } \mathcal{P}_2 \to 0, \quad [\mathcal{U}_2 \text{ and } \mathcal{P}_2] \text{ continuous,} \\ \qquad\qquad\qquad \mathcal{U}_2, \mathcal{V}_2 \text{ and } \mathcal{P}_2 \to 0 \end{array} \Bigg\}, \quad (3.14)$$

where x_0 is the point where the interface intersects the free surface.

Eqs. (3.7) and (3.8) allow $\mathcal{U}_j$ and $\mathcal{V}_j$ to be expressed as linear functions of $\mathcal{P}_j$ and $d\mathcal{P}_j/dx$, i.e.,

$$\mathcal{U}_j = -i[\mathcal{P}_{jx}(\sigma + k\bar{V}_j) + fk\mathcal{P}_j]$$
$$\div \bar{\rho}[f(f + \bar{V}_{jx}) - (\sigma + k\bar{V}_j)^2], \quad (3.15)$$

$$\mathcal{V}_j = [\mathcal{P}_j k(\sigma + k\bar{V}_j) + (f + \bar{V}_{jx})\mathcal{P}_{jx}]$$
$$\div \bar{\rho}[f(f + \bar{V}_{jx}) - (\sigma + k\bar{V}_j)^2]. \quad (3.16)$$

Substitution of these expressions in (3.10) and (3.11), followed by elimination of $\mathcal{3C}$ by means of (3.12) results in two equations for $\mathcal{P}_1$ and $\mathcal{P}_2$, i.e.,

$$F_1(x)\mathcal{P}_{1xx} + F_2(x)\mathcal{P}_{1x} + F_3(x)\mathcal{P}_1 = F_4(x)(\mathcal{P}_1 - \mathcal{P}_2), \quad (3.17)$$

$$G_1(x)\mathcal{P}_{2xx} + G_2(x)\mathcal{P}_{2x} + G_3(x)\mathcal{P}_2 = G_4(x)(\mathcal{P}_2 - \mathcal{P}_1), \quad (3.18)$$

where the variable coefficients are defined as follows:

$$\left. \begin{array}{l} F_1(x) = -(H_T - \bar{h}_I) \\ F_2(x) = -F_1(x)[f\bar{V}_{1xx} - 2(\sigma + k\bar{V}_1)k\bar{V}_{1x}] \\ \qquad\qquad \times [f(f + \bar{V}_{1x}) - (\sigma + k\bar{V}_1)^2]^{-1} + \bar{h}_{Ix} \\ F_3(x) = -F_1(x)k^2 + kfF_2(x)(\sigma + k\bar{V}_1)^{-1} \\ F_4(x) = g'^{-1}[f(f + \bar{V}_{1x}) - (\sigma + k\bar{V}_1)^2] \end{array} \right\}, \quad (3.19)$$

$$\left. \begin{array}{l} G_1(x) = -(h_B - \bar{h}_I) \\ G_2(x) = -(h_B - \bar{h}_I)_x \\ G_3(x) = -G_1(x)k^2 - fkG_2(x)/\sigma \\ G_4(x) = g'^{-1}(f^2 - \sigma^2) \end{array} \right\}. \quad (3.20)$$

If $\bar{h}_I$ were a linear function of x, then $\bar{V}_j$ would be a constant, and the system (3.10) and (3.11) would reduce to the appropriate equations used earlier in an atmospheric frontal model (Orlanski, 1968, hereafter referred to as FM068).

It is convenient to define some dimensionless parameters:

$$\text{Ro} = \mathcal{V}/(L_s f); \quad \tau = \sigma/(k\mathcal{V}); \quad \text{Ri} = g'H_T/\mathcal{V}^2; \quad \mu = kL_s$$

where Ro is the Rossby number based on the shear of the unperturbed flow, τ the negative of the phase velocity divided by the shear, Ri the Richardson number, and μ the dimensionless wavenumber. The coefficients defined in (3.19) and (3.20) thus become

$$\left. \begin{array}{l} F_1(x) = -\left[1 - h_0 - \dfrac{1}{\text{RoRi}}(1+x)e^{-x}\right] \\[2ex] F_2(x) = -F_1(x)\dfrac{[(x-2) - 2(\text{Ro}\mu)^2(\tau + xe^{-x})(1-x)]\text{Ro}e^{-x}}{[1 + \text{Ro}(1-x)e^{-x} - (\text{Ro}\mu)^2(\tau + xe^{-x})^2]} - \dfrac{xe^{-x}}{\text{RoRi}} \\[2ex] F_3(x) = -\mu^2 F_1(x) + F_2(x)/\text{Ro}(\tau + xe^{-x}) \\[1ex] F_4(x) = [1 + \text{Ro}(1-x)e^{-x} - (\text{Ro}\mu)^2(\tau + xe^{-x})^2]/\text{RiRo}^2 \end{array} \right\}, \quad (3.21)$$

$$\left. \begin{array}{l} G_1(x) = -[h_B - h_0 - (1+x)e^{-x}/(\text{RoRi})] \\[1ex] G_2(x) = -xe^{-x}/(\text{RoRi}) - h_{Bx} \\[1ex] G_3(x) = -\mu^2 G_1(x) + G_2(x)/(\text{Ro}\tau) \\[1ex] G_4(x) = [1 - (\text{Ro}\mu\tau)^2]/\text{RiRo}^2 \end{array} \right\}, \quad (3.22)$$

where h_0 and h_B are now defined, respectively, as the amplitude of the interface at $x \rightarrow \infty$ and the height of the bottom topography divided by the total height H_T.

The boundaries conditions for Region I are:

$$x=0, \qquad x=E_b \rightarrow \infty$$
$$\mathcal{P}_{1x}=-\mathcal{P}_1/(\mathrm{Ro}\tau), \quad \mathcal{P}_1=0 \qquad \Big\} \qquad (3.23)$$
$$\mathcal{P}_{2x}=-\mathcal{P}_2/(\mathrm{Ro}\tau), \quad \mathcal{P}_2=0$$

For Region I (side rigid wall) we now have the two second-order equations, (3.17) and (3.18), with the four homogeneous boundary conditions for the variables $\mathcal{P}_1$ and $\mathcal{P}_2$. Since we are interested in complex values of τ, we expect $\mathcal{P}_1$ and $\mathcal{P}_2$ to be complex.

We have explored the solutions of this system by a numerical method (FM068) for the ranges $20 \leq \mathrm{Ri} \leq 80$, $0.1 \leq \mathrm{Ro} \leq 0.5$, $0.4 \leq h_0 \leq 0.8$; primary emphasis has been placed on the nonreal values of $\tau = \tau_r + i\tau_i$.

Because of the range of variation of the many parameters involved in this system, we consider it convenient to present the results in two parts. In Case A we are interested in the stability of an atmospheric polar jet. In particular, we are interested in the westerly flow over Antarctica where there is a strong variation in topography. The stability of this jet will be examined through the use of the two-layer model, assuming a rigid wall at a latitude close to the pole. This is characterized by two layers of nearly equal depth separated by an interface with a variable slope as a function of Ri. We consider small values of Ro with and without bottom topography.

In Case B we will consider the case in which the parameters and the bottom topography are similar to the Gulf Stream.

4. The unstable mode

a. Case A

With a constant value of Rossby number (Ro$=0.1$) and varying the Richardson number ($20 \leq \mathrm{Ri} \leq 80$), the eigenvalues τ and the eigenfunctions $\mathcal{P}_j$ were computed for the case in which the interface divides both layers nearly equally ($h_0=0.4$).

Fig. 3 shows isolines of the time $[T_D = \ln 2/(4\pi\mu\mathrm{Ro}\tau_i)$; in pendulum days, $4\pi/f]$ for the disturbance to double its amplitude as a function of the shear of the mean flow ($\mathcal{V}/H_T$) and a dimensionless wavelength $L_y/L_s = 2\pi/\mu$. The variability of V/H_T is a result of modifying the Richardson number and keeping $(\rho_2-\rho_1)/\bar{\rho}=2\times10^{-1}$ and $H_T=8\times10^3$ m. With $\mathcal{V}/H_T=2$ m sec^{-1} km^{-1}, $\mathcal{V}=16$ m sec^{-1}, and the horizontal scale fixed at $L_s=\mathcal{V}/ (f\mathrm{Ro})=1.6\times10^6$ m, the most unstable waves for this shear of the mean flow corresponds to wavelengths of the order $L_y/L_s=4$, so that $L_y=6400$ km. We can see that when $2\pi/\mu>1$, the system becomes unstable, equivalent to Eady's (1949) results.

The dashed lines in Fig. 3 indicate the growth time T_D where there is a small bottom topography (in this case bottom topography is $h_B = h_2 e^{-x}$ where $h_2=0.05$).
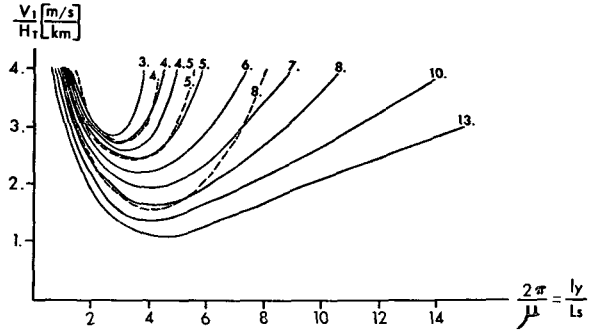

Fig. 3. Contour lines of the time T_D, in days, required to double the wave amplitude are shown as a function of the mean shear and the wavelength. The dashed lines correspond to the case with bottom topography, solid lines to the case without bottom topography.

We note a small influence for medium wavelengths but a remarkable effect for larger wavelengths. The isoline $T_D=8$ pendulum days for which $2\pi/\mu \leq 5.5$ is more or less the same with or without bottom topography. However, in the case $2\pi/\mu>5.5$, the system becomes more stable with increasing bottom slope. We can identify this effect as similar to the β-effect which stabilizes the longer wavelengths (Charney, 1947). The stabilizing effect of the bottom topography was also pointed out by Pedlosky (1964) in his analysis of the stability of a two-layer system with a small bottom topography. He concluded from the necessary condition of instability that a slope in the bottom topography will work as a stabilizing mechanism. It will be shown here, for cases in which the slope of the bottom topography is a stabilizing factor, that the amplitude of the bottom topography is a destabilizing factor where it appears as a coefficient. It is the amplitude of the bottom topography related to the vertical shear by $\bar{V}_g=\bar{V}_1/(H_T-h_B)$ which is the destabilizing factor. The combination of both slope and amplitude of the bottom topography may or may not force the system to become more stable. We will show this in two simple experiments. In the upper part of Fig. 4 the imaginary part of the eigenvalue of τ is shown as a function of $h_B(0)$ with Ri$=30$, Ro$=0.1$, $h_0=0.6$ and $\mu=0.8$. This imaginary part τ_i decreases where $h_B(0)$ increases and the system becomes more stable. The relative position of the interface and the bottom topography is shown in the lower part of Fig. 4. Fig. 5 shows τ_i as a function $h_B(0)$, $h_B(x)$ being a tangent hyperbolic function of x. Now τ_i increases with increasing $h_B(0)$, and the system becomes more unstable. There is no contradiction between the two results, if we remember that $\bar{V}_1(x)$ has a maximum at $x=1$. The perturbed motion also has a maximum at $x=1$, and decays exponentially for larger x. In Fig. 4 the amplitude of the bottom topography increases below the jet, but the effect of the large bottom slope is much more important. Consequently, the perturbation motion becomes three dimensional and the increased static stability is more important than the increase of
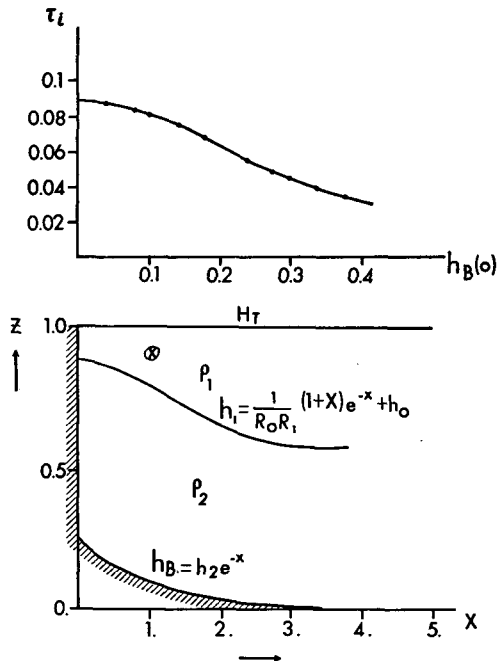
FIG. 4. The upper graph shows the variation of the absolute value of the imaginary part of τ vs the maximum amplitude of the bottom topography. The lower graph shows the corresponding bottom topograph where $\otimes$ denotes the position of the jet center.

the vertical shear. The result is a stabilizing effect. In the second case (Fig. 5) the result is quite different. Below the jet $(x=1)$ the slope of the bottom topography is relatively small and the depth of the lower layer $[H_T - h_B(1)]$ is also relatively small compared to the
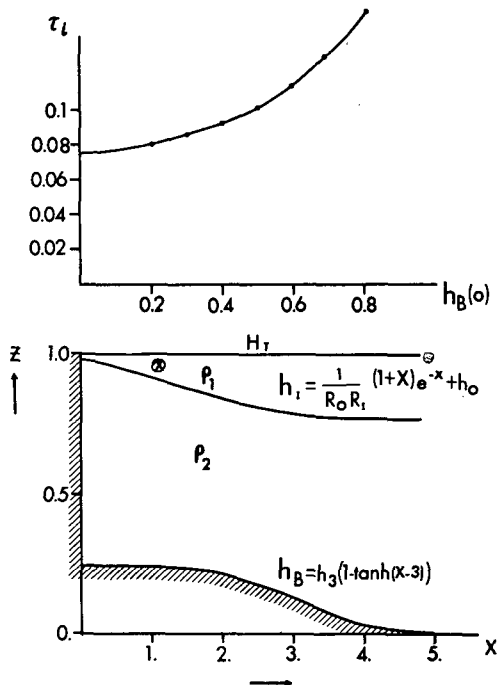
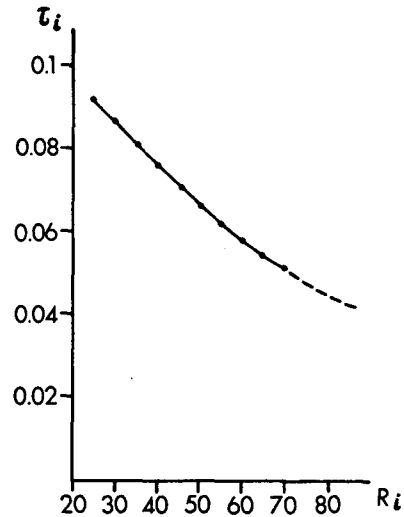FIG. 5. Same as Fig. 4, except for different bottom topography.

FIG. 6. The absolute value of τ_i, computed with Ro$=0.1$ and $\mu=0.8$, without bottom topography, is shown as a function of the Richardson number.

previous example. The vertical shear is much more important now in destabilizing the system. It is true that for $x=3$ the slope is large, but in this region, as mentioned before, the disturbed motion for large x is weak. The stabilizing effect near $x=3$ is not great enough to oppose the increased instability in the region of maximum baroclinicity near $x=1$; overall the system becomes more unstable. We must expect from these results that the bottom topography will indeed play an important role in the energetics and kinematics of unstable waves which occur in jets flowing over steep bottom topography.

The behavior of τ_i as a function of Ri without bottom topography is shown in Fig. 6 for a particular wavenumber $\mu=0.8$ and Ro$=0.1$. Here τ_i is a decreasing function of Ri which, in fact, is a parameter involving only the ratio of static stability and the baroclinicity of the mean flow.

To show that the two-layer system contains the same features for baroclinic waves as the continuously stratified model, we may go back to a simple example. If one allows a sinusoidal variation in Eady's model (see Phillips, 1963, pp. 145–150) with the flow bounded by walls at $x=0$ and $x=L_E$, the criterion for instability, when $k=0$, can be written as

$$\frac{gH_T}{f^2}\left(\frac{\Delta\rho}{\bar\rho}\right)\frac{m^2\pi^2}{L_E^2} < (2.3994)^2,$$

where m is the number of half wavelengths between $x=0$ and $x=L_E$, and $\Delta\rho$ is the density difference from $z=0.75H_T$ to $z=0.25H_T$ in Eady's Boussinesq fluid. A complete analogy occurs in a two-layer system with a steep slope in the interface. One may make the conjecture that as L_E increases (Ri increases in the frontal case due to the relation between Ri and L_E from Mar-

gules' formula) additional unstable roots will appear, and these will have shorter "wavelengths" in the x direction than those unstable roots which have already appeared. Their growth rates will also be less (FM068, p. 184).

In this model the horizontal scale is involved only in Ro. The appearance of additional unstable roots when L_E is increased is illustrated in Fig. 7, constructed for Ri=30, $h_B(0)=0$, $\mu=0.8$. When Ro=0.3 an unstable root will appear. When Ro decreases, this root increases, allowing a new root to appear. This new root is always maintained below the first one. Fig. 8 shows one of the eigenfunctions for roots I and II for the case Ro=0.2. The new root has a higher wavenumber in the x direction, confirming the previous conjecture.

b. Case B

In view of the results of the previous section in which the stability of a jet depends on the kind of topography over which it flows, we are encouraged to attempt an application of the theory to the case of the Gulf Stream.

Fig. 9 shows the geographic position of the axis of the Gulf Stream (heavy line) and the contours of the bottom topography (thin lines). Notice that the stream is parallel to the contour lines over two regions from 28N to about 35N (Region I) and then again above 36N (Region II). Near Cape Hatteras (35.5N), however, the jet crosses a strong slope downstream. Our model will not apply to this region because we assume in the model that the bottom topography has no variation in the direction of the jet.
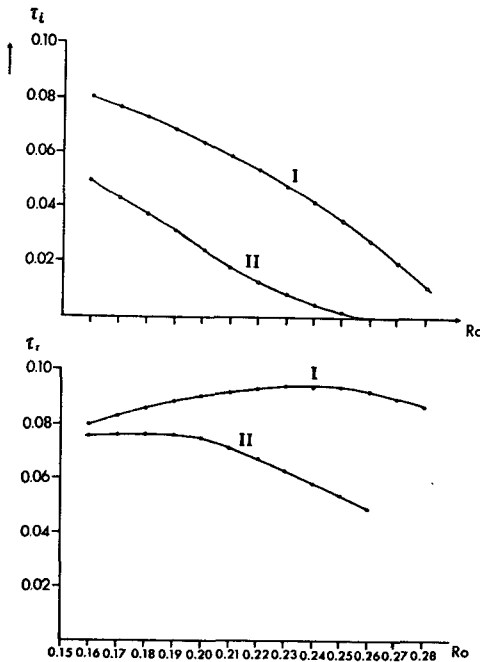
FIG. 7. In the upper part the absolute value of τ is shown as a function of the Rossby number (Ri=30, $\mu=0.8$, no bottom topography). The two roots are indicated by I and II. The lower part of the graph shows τ_r vs Ro.
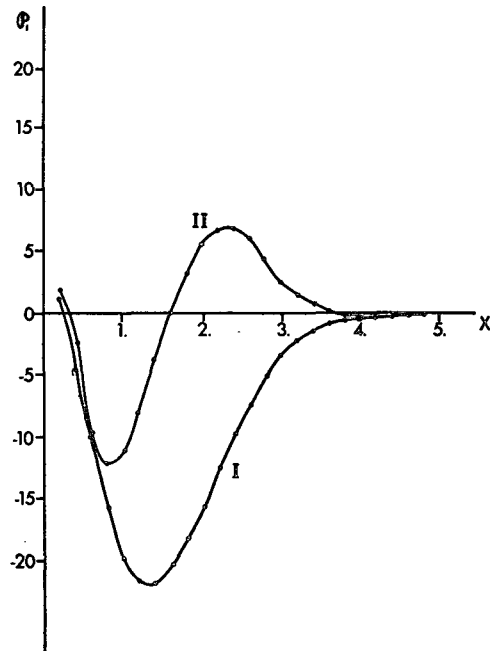
FIG. 8. The eigenfunctions $\mathcal{P}_1$, corresponding to roots I and II at Ro=0.2, are shown as a function of X.

Before going into the details of previous stability studies of the Gulf Stream we will briefly mention some theories connected with the meandering behavior. There are two main ideas to explain this phenomenon: 1) the Gulf Stream is a free jet controlled by the bottom topography, and 2) the Gulf Stream is an unstable jet.

Warren (1963) has investigated the effects of topography on the Gulf Stream north of Cape Hatteras (Region II). He shows that the current, a free jet in the region, can indeed be controlled by the topography. Warren also shows that the meanders of the Gulf Stream can result from depth variation and that they are an inherent feature of a steady-state theory. The steady theory may be applied to the actual time dependent case if the changes are of low frequency. That is to say, conditions at the entrance region must change slowly enough to provide time for the flow to achieve a near steady state before the entrance condition substantially changes. As pointed out by Greenspan (1963), the exact causes of the slow oscillation in the initial position of the meander pattern are unknown; there may be some kind of instabilities connected with them. Extending Warren's ideas, Robinson and Niiler (1967) considered a baroclinic jet and obtained quite good agreement with some observations. Even if we recognize that quasi-steady finite waves are well described from these theories, the fact that meanders south of Cape Hatteras and meanders with considerable time dependence are not described by the above theories, shows, we feel, that some other dynamic process is involved in the formation and posterior development of the meanders in the Gulf Stream.
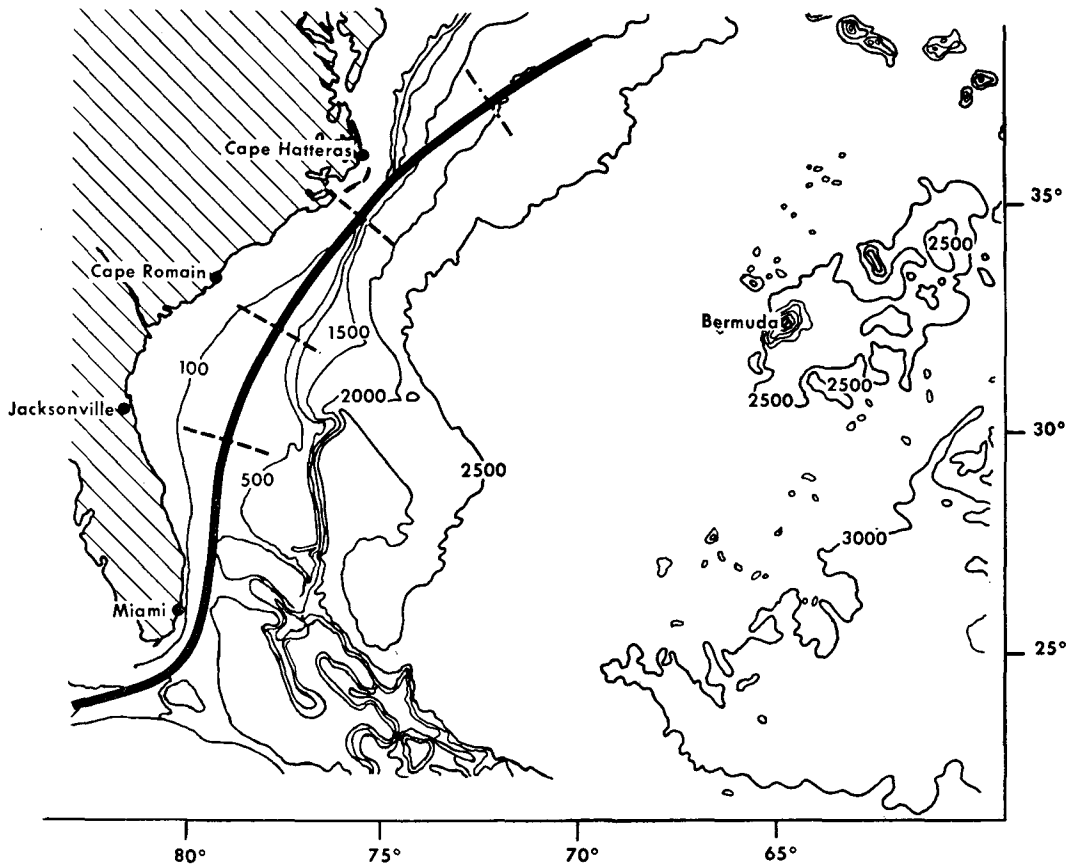
FIG. 9. The geographical position of the mean axis of the Gulf Stream is shown by the heavy solid line among the bottom contours. The dashed line indicates Region I. The dashed-dotted line indicates Region II.

In the second group, as previously mentioned, there are few theories based on stability analysis because of the mathematical complexity of the nonconstant coefficients in the differential equations when considering the interaction of both layers. As we see in (3.17)–(3.18) this feature makes it impossible to make a complete study from an analytical point of view. Many authors (Stommel, 1953; Stern, 1961; Lipps, 1963) studied a simpler model considering only the dynamically active upper layer. Duxbury (1963) considered a two-layer model but had no interaction between the layers.

We will show now that this simplification not only neglects the effect of the bottom topography in the solutions, but also changes the character of the possible instabilities that may occur in a two-layer system. For this purpose let us consider the simpler case of quasi-geostrophic perturbations in a two-layer system. Accordingly, we must rewrite the expressions defined in (3.21)–(3.22) so that only that part which is of first order with respect to the Rossby number is retained. The conditions for the validity of this simplified model are Ro$\ll$1 and Ri$\sim$O(Ro^{-2}). The latter condition is needed to assume that the slope of the interface given by (RiRo)$^{-1}$ will be of the O(Ro). The corresponding

coefficients are:

$$
\left.
\begin{aligned}
F_1 &= -(1-h_0)+O(\text{Ro}) \\
F_2 &= O(\text{Ro}) \\
F_3 &= \mu^2(1-h_0)+\frac{(1-h_0)(x-2)e^{-x}}{(\tau+xe^{-x})} \\
&\qquad\qquad\qquad -\frac{xe^{-x}}{\text{Ro}^2\text{Ri}(\tau+e^{-x})} \\
F_4 &= \frac{1}{\text{Ro}^2\text{Ri}}+O(\text{Ro})
\end{aligned}
\right\}, \qquad (4.1)
$$

$$
\left.
\begin{aligned}
G_1 &= -(h_B-h_0) \\
G_2 &= -h_{Bx} \\
G_3 &= \mu^2(h_B-h_0)-\frac{xe^{-x}}{\text{Ro}^2\text{Ri}}\frac{h_{Bx}}{\text{Ro}}+O(\text{Ro}) \\
G_4 &= \frac{1}{\text{Ro}^2\text{Ri}}+O(\text{Ro})
\end{aligned}
\right\}. \qquad (4.2)
$$

We must limit the bottom slope so that it will also be consistent with the quasi-geostrophic assumption. This requires that $h_{Bx} \sim O(\text{Ro})$ and that the term h_{Bx}/Ro in G_3 is of the order of unity. Rewriting the system (3.17)–(3.18) to the first order in Ro we have

$$F_1 \mathcal{P}_{1xx} + F_3 \mathcal{P}_1 = F_4(\mathcal{P}_2 - \mathcal{P}_1), \qquad (4.3)$$

$$G_1 \mathcal{P}_{2xx} + G_3 \mathcal{P}_2 = G_4(\mathcal{P}_2 - \mathcal{P}_1), \qquad (4.4)$$

with the boundary conditions

$$\left. \begin{array}{ll} x = 0, & x \to \infty \\ \mathcal{P}_1 = \mathcal{P}_2 = 0, & \mathcal{P}_1 = \mathcal{P}_2 \to 0 \end{array} \right\}. \qquad (4.5)$$

If (4.3) is multiplied by the complex conjugate of $\mathcal{P}_1$ and (4.4) by the complex conjugate of $\mathcal{P}_2$, and the results, integrated with respect to x over the interval $0 < x < \infty$, are then subtracted from one another, we have

$$\int_0^\infty [F_1 |\mathcal{P}_{1x}|^2 - G_1 |\mathcal{P}_{2x}|^2 + F_3 |\mathcal{P}_1|^2 - G_3 |\mathcal{P}_2|^2] dx$$

$$= -\int_0^\infty [F_4(|\mathcal{P}_2|^2 + |\mathcal{P}_1|^2) + F_4 \text{Real}(\mathcal{P}_1 \mathcal{P}_2)] dx. \quad (4.6)$$

Since only F_3 and G_3 are complex, we have the condition that

$$\text{I}_{\text{mag}} \int_0^\infty [F_3 |\mathcal{P}_1|^2 - G_3 |\mathcal{P}_2|^2] dx = 0. \qquad (4.7)$$

Combining (4.1), (4.2) and (4.7), we have

$$\tau_i \int_0^\infty \left\{ \left[F_1(x-2)e^{-x} + \frac{xe^{-x}}{\text{Ro}^2 \text{Ri}} \right] \frac{|\mathcal{P}_1|^2}{|\tau + xe^{-x}|^2} \right.$$

$$\left. - \left[\frac{xe^{-x}}{\text{Ro}^2 \text{Ri}} + \frac{h_{Bx}}{\text{Ro}} \right] \frac{|\mathcal{P}_2|^2}{|\tau|^2} \right\} dx = 0. \quad (4.8)$$

If $\tau_i \neq 0$, the integrand in (4.8) must be zero, i.e.,

$$\int_0^\infty \left\{ q_{1x} \frac{H_1 |\mathcal{P}_1|^2}{|\tau + xe^{-x}|^2} + q_{2x} \frac{H_2 |\mathcal{P}_2|^2}{|\tau|^2} \right\} dx = 0.$$

Here $q_{1x} H_1$ and $q_{2x} H_2$ are:

$$q_{1x} H_1 = F_1 V_{1xx} + \frac{(V_1 - V_2)}{\text{Ro}^2 \text{Ri}} = F_1(x-2)e^{-x} + \frac{xe^{-x}}{\text{Ro}^2 \text{Ri}},$$

$$q_{2x} H_2 = F_2 V_{2xx} + \frac{(V_2 - V_1)}{\text{Ro}^2 \text{Ri}} - \frac{h_{Bx}}{\text{Ro}} = \frac{h_{Bx}}{\text{Ro}} - \frac{xe^{-x}}{\text{Ro}^2 \text{Ri}}.$$

A necessary condition for instability is that q_{1x} and q_{2x} have opposite signs. A similar contition for a quasi-geostrophic two-layer model was derived by Pedlosky (1964). If $q_{1x} > 0$, the necessary condition for instability

is $\bar{V}_1 > 0$, allowing a baroclinic instability. However, if in (4.3) we neglect the dynamics of the lower layer, $\mathcal{P}_2$ is zero and the necessary condition of instability is that q_{1x} must change sign, consistent with the Stern and Lipps criteria. This is possible due to the horizontal shear of the flow producing a barotropic type of instability. Therefore, the assumption made in the previous works of neglecting the dynamics of the lower layer allows only one type of instability and therefore may not be appropriate to describe the meandering process in the Gulf Stream.

Now we are able to present our results. The characteristic parameters for the Gulf Stream are as follows: $H_T(1 - h_0)$, the depth of the upper layer is, 1000 m, and the total depth H_T is ~ 5000 m. The ratio of density difference $\Delta \rho / \rho$ is 2×10^{-3}, the horizontal scale L_s is 50 km, and the maximum amplitude of the jet $(\mathcal{V})$ is 1.5 m sec^{-1}. With these values the range of Ri and Ro are: $20 \leq \text{Ri} \leq 80$, and $0.2 \leq \text{Ro} \leq 0.5$.

Fig. 6 in the previous section shows the behavior of τ_i as a function of Ri. Here we will only look at Ri = 20 or 30.

Before going into the details of the analysis, we will briefly describe the general characteristics of regions shown in Fig. 9. Region I is characterized by a bottom topography varying from a few hundred to a few thousand meters in depth over a lateral distance of < 200 km. The interface is always below the free surface and bounded in the horizontal by a wall at $x = 0$. In Region II the bottom below the jet is about 4000 m deep and the interface intersects the free surface.

5. Analysis of the two regions

a. Region I

Fig. 10 shows τ vs the dimensionless wavenumber μ for a constant Ri = 30, Ro = 0.3, $h_0 = 0.79$, and the bottom topography $h_B = h_3[1 - \tanh(x-3)]$, where $h_3 = 0.35$, and h_3 is such that for $x = 0$, $h_B(0)$ is 0.7. In the upper part of Fig. 10 τ_i is plotted as a function of μ. A monotonic decrease of τ_i with the wavenumber μ is shown; $\tau_i \simeq 0$ evidently occurs approximately at $\mu \simeq 2.2$. In the lower part of Fig. 10 the dimensionless phase velocity τ_r is shown as a function of μ, having a smooth maximum for $\mu = 1.6$. Note that the growth rate is $\tau_i = \text{Ro} \mu \tau_i f$, and (for $f = 10^{-4}$ sec^{-1}) the maximum occurs with $\tau_{i\max} = 2.3 \times 10^{-6}$ sec^{-1}, $\mu = 1.4$. The wavelength corresponding to this maximum is $L_y = (2\pi/\mu) L_s = 220$ km and the period of the most unstable wave is $T_p = (2 \text{Ro} \mu \tau_r)^{-1} (4\pi/f) = 10.02$ days.

The variation of $\mathcal{T}$ with Ro (Ro is the ratio between the shear and earth vorticity) for a constant wavelength, corresponding to $\mu = 1.8$, Ri = 20 and $h_B(0) = 0.6$, is shown in Fig. 11. As before, the ordinate in the upper part shows τ_i but the abscissa is now Ro. We can see that τ_i decreases when Ro increases; the lower graph of τ_r vs Ro shows a maximum for Ro = 0.315.
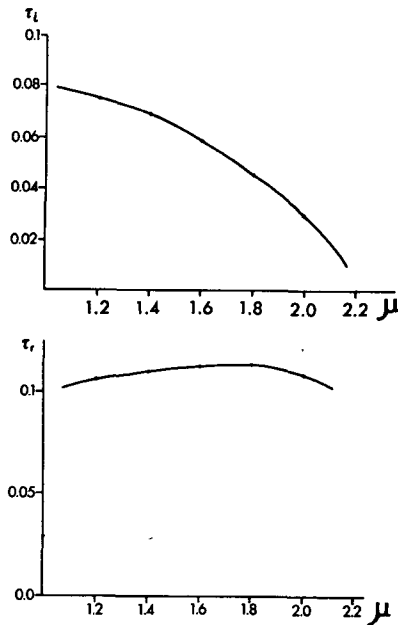
Fig. 10. The upper part of the graph shows τ_i vs the wavenumber μ for Ri=30, R_0=0.3, bottom topography as described in text. The lower part of the graph shows τ_r.

Fig. 12. The variation of τ_i (upper graph) and τ_r (lower graph) as a function of the position of the maximum slope of the bottom topography for $h_B=h_3[1-\tanh(x-\kappa)]$, $\mu=1.8$, Ro=0.25, Ri=20, $h_0=0.79$.

Fig. 12 shows the variation of τ when the position of the maximum shape of the bottom topography is changed. The parameters $\mu=1.8$, Ro=0.25, Ri=20, $h_0=0.79$ are held fixed and two different amplitudes of the bottom topography (0.6 and 0.7) are considered. The shape of the bottom topography is given by $h_B=h_3[1-\tanh(x-\kappa)]$.

The position of the jet is at $x=1$. We notice that for κ (position where the maximum slope appears) larger than 5, τ remains practically constant. Again, it is possible

to see that for larger amplitudes of bottom topography the system is more unstable.

Fig. 13 shows the behavior of τ when introducing a bottom topography of the type $h_B=h_2e^{-x}$

Fig. 11. The upper graph shows the variation of the imaginary part of τ as a function of the Rossby number Ro for Ri=20, $\mu=1.8$, bottom topography as described in text. The lower graph shows the variation of the real part of τ.
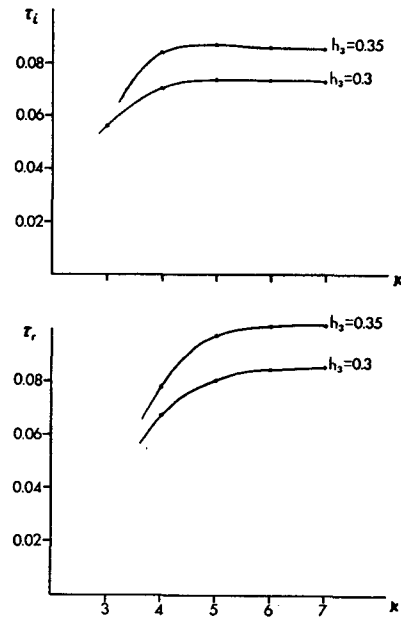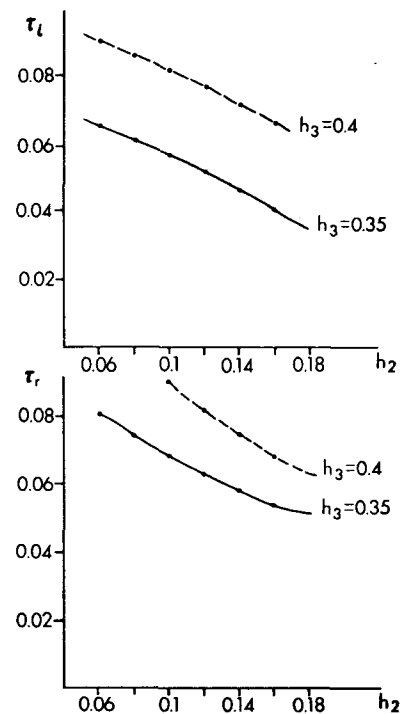

Fig. 13. The variation of the imaginary and real part of τ when the amplitude of the bottom topography is changed $\{h_B=h_2e^{-x}+h_3[1-\tanh(x-5)]$, Ro=0.3, Ri=20, $\mu=1.8$, $h_0=0.8\}$.

$+h_3[1-\tanh(x-5)]$. The fixed parameters this time are Ro$=0.3$, Ri$=20$, $\mu=1.8$, $h_0=0.8$. Cases I and II correspond to $h_3=0.35$ and $h_3=0.4$. Here τ_i and τ_r decrease when $h_B(0)\simeq(h_2+2h_3)$ increases. It is clear that the system becomes more stable now because of the influence of increasing the slope of the bottom topography below the jet. Case II is more unstable than Case I because Case II has a larger mean value of the amplitude of the bottom topography.

b. Region II

In this case $-\infty \leq x \leq \infty$ and the interface intersects the free surface at $x=x_0[\bar{h}_I(x_0)=1]$, which is a singular point for the differential equations (3.17) and (3.18). In order to find the eigenvalues for this case we must divide the region into two zones: Zone A, $-\infty \leq x \leq x_0$, in which we consider a single barotropic nondivergent layer with a constant bottom topography (Fig. 2), and Zone B, defined by $x_0 \leq x \leq \infty$. As in the previous case this is a two-layer system with a variable bottom topography. In Zone A there is a nondivergent field allowing analytical solution of the pressure field of the form

$$\mathcal{P}_2=\mathcal{P}_2(x_0)e^{k(x-x_0)}, \qquad (5.1)$$

satisfying the boundary condition in $x=-\infty$. For matching the solutions of Zone A and Zone B we must satisfy continuity at $x=x_0$ of the normal velocity U_2, the pressure $\mathcal{P}_2$, and finiteness of $\mathcal{P}_1$, $\mathcal{U}_1$ and $\mathcal{V}_1$. From (3.14) the boundary conditions are

$$\left.\begin{array}{c}\mathcal{P}_{2x}=k\mathcal{P}_2\\ \mathcal{P}_1 \text{ and } \mathcal{P}_{1x} \text{ finite}\end{array}\right\} \text{ at } x=x_0. \qquad (5.2)$$

We used the same system as in the general case for computing τ and the eigenfunction, but instead of starting from $x=0$, we start from $x=X_0$ with the boundary conditions (5.2). We must point out that all parameters defined before have the same meaning, except Ro$=\mathcal{V}/(L_sf)$, which was defined as the ratio between the horizontal shear and Coriolis parameter. It is evident from Fig. 2 that the horizontal length is $L_s^*=(1-x_0)L_s$ and the new Rossby number is given as Ro$^*=$Ro$/(1-x_0)$ and, of course, this will become physically important, keeping Ro as the relevant parameter in our model.

Fig. 14 shows the behavior of τ vs the wavenumber μ for Ri$=30$, $h_0=0.8$, $h_3=0.05$ and Ro$^*=0.46$. In this case $x_0=0.7$, τ_i has a maximum at $\mu\sim1.4$, and τ_r increases with μ. [For the case Ro$^*=0.46$, Ro will be given by $(1-x_0)$Ro$^*=0.138$, corresponding a horizontal scale L_s of 120 km. Here τ_i has a maximum of 1.6×10^{-6} sec^{-1} at $\mu=2.2$, corresponding to a wavelength $L_y=365$ km and period $T_p=37.42$ pendulum days.] Comparing with values computed in Region I ($T_p=10.02$ pendulum days and $L_y=220$ km), we notice that there is a significant increase in the period and the wavelength of the most unstable waves. Physically, the variation of the
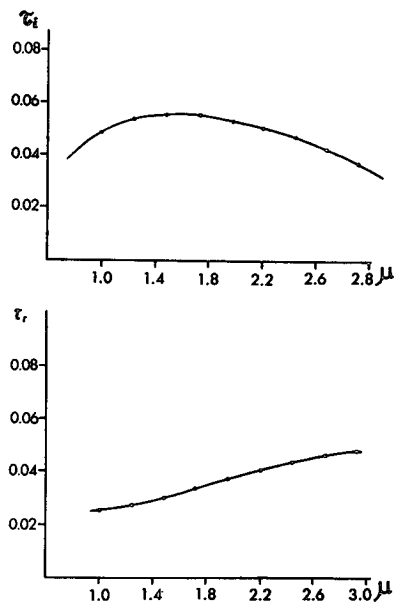

FIG. 14. The absolute value of τ_i and the real part of τ as a function of the wavelength μ (Ri$=30$, Ro$^*=0.46$, bottom topography as described in text.).

bottom topography in Region I probably selects shorter wavelengths due to the large vertical velocity in these waves (in opposition to Region II where the waves are quasi-geostrophic) and the plane of the wave is more quasi-horizontal, allowing much longer wavelengths.

6. Energy transformation

The energy equation for this model can be derived in the same way as in the frontal case (FM068) from the fundamental equations (2.1)–(2.4). The procedure is multiplication of (2.1) with $\rho_1(H_T-h_I)\mathbf{V}_1$ for $J=1$ and $\rho_2(h_I-h_B)\mathbf{V}_2$ for $J=2$, followed by addition of (2.3), (2.4) multiplied by $\frac{1}{2}\rho_J|\mathbf{V}_J|^2$. This gives

$$\frac{\partial}{\partial t}\left[\rho_1(H_T-h_I)\frac{|\mathbf{V}_1|^2}{2}+\rho_2(h_I-h_B)\frac{|\mathbf{V}_2|^2}{2}\right]$$

$$=-\nabla\cdot\left[(H_T-h_I)\left(p_1+\rho_1\frac{|\mathbf{V}_1|^2}{2}\right)\mathbf{V}_1\right.$$

$$\left.+(h_I-h_B)\left(p_2+\rho_2\frac{|\mathbf{V}_2|^2}{2}\right)\mathbf{V}_2\right]$$

$$+p_1\nabla\cdot\mathbf{V}_1(H_T-h_I)+p_2\nabla\cdot\mathbf{V}_2(h_I-h_B). \qquad (6.1)$$

The boundary conditions are cyclic continuity in y and that u vanish at $x=0$ and $x=\infty$ for Region I and at $x=-\infty$ and $x=\infty$ for Region II. An area integral over a wavelength in y and over $\delta\leq x\leq\infty$ (where $\delta=0$ or $-\infty$, for Region I or II) will be denoted simply

$$\int(\quad)da.$$

Thus

$$\frac{\partial}{\partial t}\int\left[\rho_1(H_T-h_I)\frac{|\mathbf{V}_1|^2}{2}+\rho_2(h_I-h_B)\frac{|\mathbf{V}_2|^2}{2}\right]da$$

$$=+\int[p_1\nabla\cdot\mathbf{V}_1(H_T-h_I)+p_2\nabla\cdot\mathbf{V}_2(h_I-h_B)]da. \quad (6.2)$$

Multiplying (2.3) and (2.4) by p_1 and p_2, respectively, and integrating we find from (3.6) that

$$g(\rho_2-\rho_1)\int h_I\frac{\partial h_I}{\partial t}da$$

$$=-\int[p_1\nabla\cdot\mathbf{V}_1(H_T-h_I)+p_2\nabla\cdot\mathbf{V}_2(h_I-h_B)]da. \quad (6.3)$$

The interpretation of (6.2) and (6.3) is obvious; the left sides represent the time rates of change of kinetic and potential energy in the system, while the right sides represent a transformation between kinetic and potential energy.

Let us denote a y average by angular parenthesis and the deviation from this average by a prime; thus,

$$\left.\begin{aligned}\langle f\rangle&=\frac{1}{L_y}\int_0^{L_y}fdy\\f'&=f-\langle f\rangle;\ \langle f'\rangle=0\end{aligned}\right\} . \quad (6.4)$$

We define

$$K_M=\tfrac{1}{2}\rho_1\int\langle H_T-h_I\rangle\langle|\mathbf{V}_1|^2\rangle da, \quad (6.5)$$

$$K_E=\tfrac{1}{2}\rho_1\int[\langle H_T-h_I\rangle\langle|\mathbf{V}_1|^2\rangle-2\langle\mathbf{V}_1\rangle\cdot\langle h_I\mathbf{V}_1\rangle]da$$

$$+\tfrac{1}{2}\rho_2\int[\langle h_I-h_B\rangle\langle|\mathbf{V}_2|^2\rangle]da, \quad (6.6)$$

$$P_M=g(\rho_2-\rho_1)\int\tfrac{1}{2}\langle h_I\rangle^2da, \quad (6.7)$$

$$P_E=g(\rho_2-\rho_1)\int\tfrac{1}{2}\langle h_I{}'^2\rangle da. \quad (6.8)$$

The sum of all four energy forms is constant, i.e.,

$$\frac{\partial}{\partial t}(K_M+K_E+P_M+P_E)=0.$$

The equations are now to be interpreted in terms of our linearized small amplitude expansion (3.1)–(3.4), K_E, P_E being of the order of ϵ_2. We must therefore allow for changes in K_M and P_M of the order of ϵ^2. That is, we

must consider the variation of $\langle\mathbf{V}_j\rangle$ and $\langle h_I\rangle$ to the order ϵ^2. Following the derivation in FM068, we substitute (3.1)–(3.5) into definitions (6.5)–(6.8) of the four energies and retain terms to the order ϵ^2. The resulting expressions are differentiated with respect to t, introducing various $\partial/\partial t$ terms in the four integrals. These $\partial/\partial t$ terms are then evaluated by substitution from the second-order (ϵ^2) expansion into the original equations (2.1)–(2.4). The result is that the four time-rates-of-change of the energies are each equal to certain energy transformation integrals, $\int W_n da$, where the W_n are:

$$W_1=\left\{\rho_1(H_T-\bar{h}_I)\bar{V}_{1x}\langle u_1v_1\rangle-\rho_1\frac{\bar{V}_{1x}{}^2}{2}\langle h_I u_1\rangle\right.$$

$$\left.-\rho_1\bar{V}_1\left[\bar{h}_{Ix}\langle u_1v_1\rangle-(H_T-\bar{h}_I)\langle v_1u_{1x}\rangle\right]\right\}, \quad (6.9)$$

$$W_2=-g(\rho_2-\rho_1)(H_T-\bar{h}_I)\bar{h}_{Ix}U_1'', \quad (6.10)$$

$$W_3=g(\rho_2-\rho_1)\bar{h}_{Ix}\langle h_I u_1\rangle, \quad (6.11)$$

$$W_4=+g(\rho_2-\rho_1)(H_T-\bar{h}_I)\langle h_I(u_{1x}+v_{1y})\rangle. \quad (6.12)$$

The time-rates-of-change of the energy integrals are:

$$\frac{\partial}{\partial t}K_M=-\int W_2da+\int W_1da, \quad (6.13)$$

$$\frac{\partial}{\partial t}P_M=-\int W_2da+\int W_3da, \quad (6.14)$$

$$\frac{\partial}{\partial t}K_E=-\int W_1da+\int W_4da, \quad (6.15)$$

$$\frac{\partial}{\partial t}P_E=-\int W_3da-\int W_4da. \quad (6.16)$$

The interpretation of these integrals is the same as in FM068. However, the inclusion in this model of a basic current varying with x has introduced extra terms in the transfer of energy by the Reynolds stresses, because $\bar{V}_{1x}\neq0$.

7. Energetics and kinematics for unstable waves along the Gulf Stream

Figs. 15–18 show in their upper left part (a) the velocity profile, the position of the interface and the bottom topography in the model chosen to correspond to the four latitudes, 29N, 31N, 33N, 37N in Fig. 9. In their upper right portion (b) five curves are plotted representing the terms W_1, W_3, and α, β, γ in (6.9). In the lower part (c) of the figures contours of the depth of the upper layer (mean plus perturbation) are shown. Values of the parameters and eigenvalues which characterize Figs. 15–19 may be seen in Table 1. The wave-
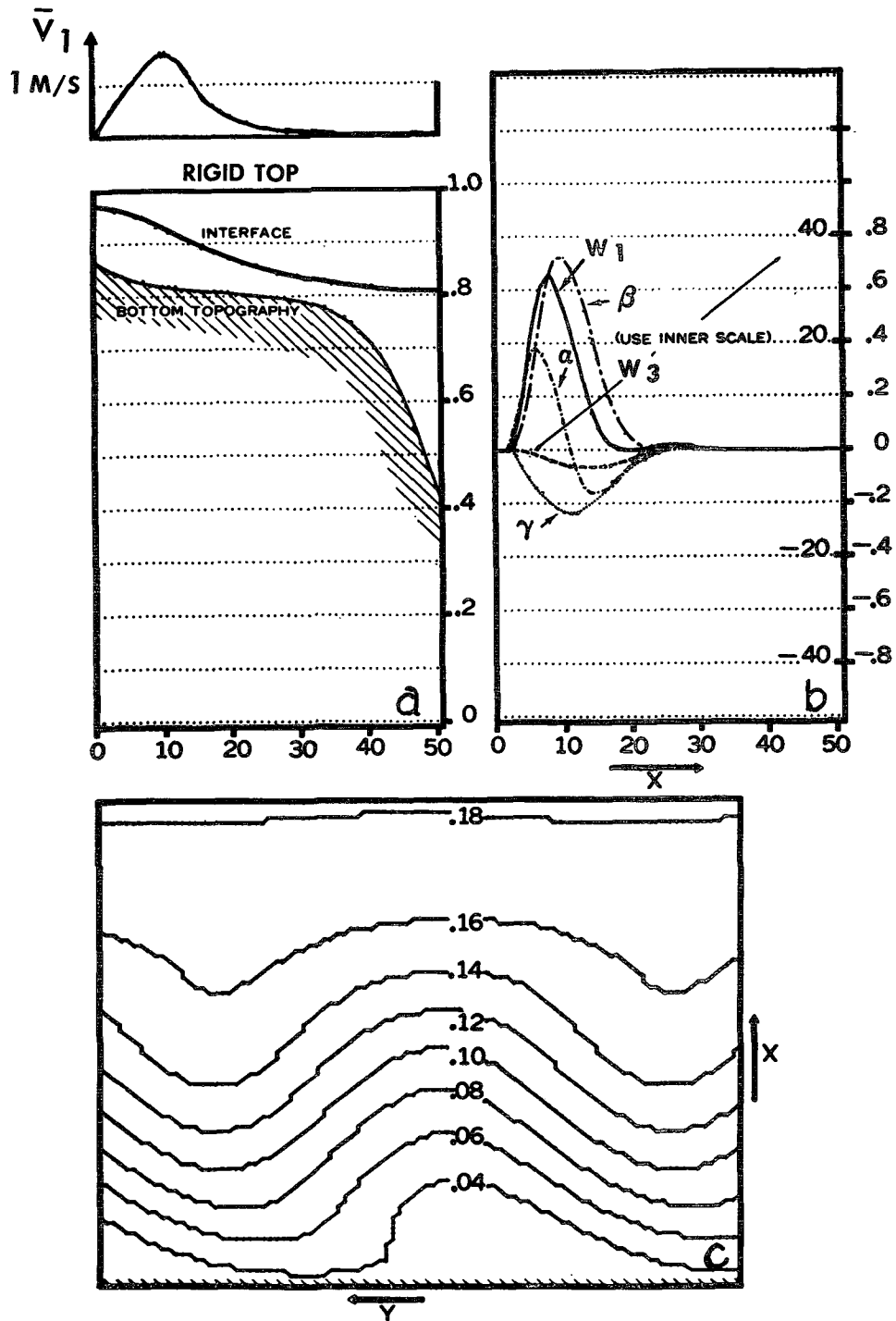
FIG. 15. Schematic position of the interface, the velocity profile, and the shape of the bottom topography at 29° latitude, a; relative magnitudes of different types of energy transfer (see text), b; and contour lines of the depth of the upper layer, $[1-h_1-He^{iku}]$, as a function of x and y, c.

number μ chosen was 1.8. This value does not correspond to the most unstable waves ($u=1.4$ in Region I, and $\mu=2.2$ in Region II) but allowed most of the dimensionless terms to be kept constant. The total height for both regions is $H_T=5000$ m. We can notice that two main

differences prevail between Regions I and II. As we mentioned previously, the wavelength and the period of the maximum unstable wave correspond to meanders observed upstream and downstream of Cape Hatteras. The growth rates of the order of a few days are con-
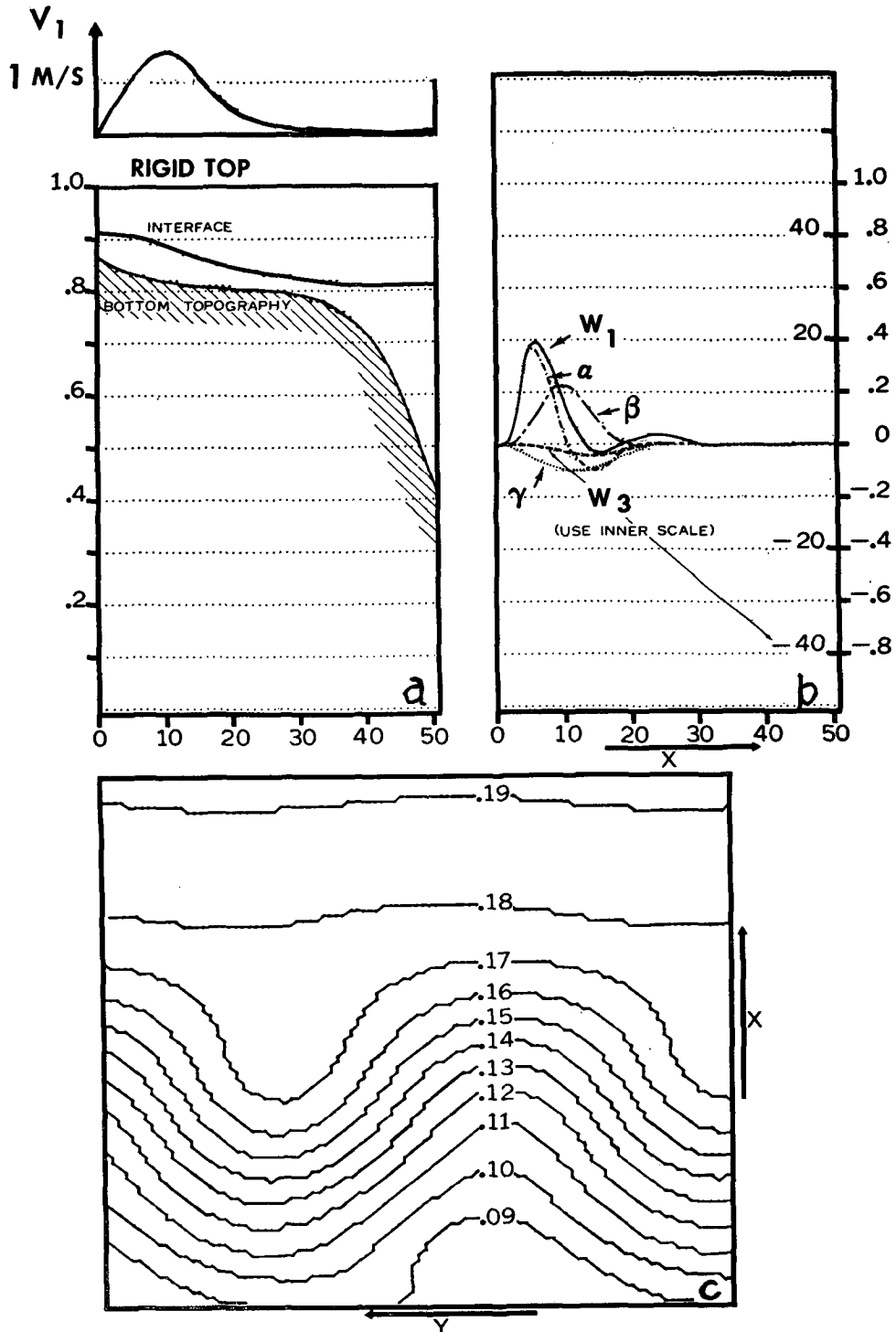
FIG. 16. Same as Fig. 15 except for 31° latitude.

siderably larger than that which is observable in meanders. However, we must remember that T_i decreases with an increase of Ro; as an example we use here Ro ~0.3 which is small compared to Ro~0.6 for the Gulf Stream and corresponds to a smaller growth rate. In addition to this, in a viscous flow the dissipative effect can become large for finite-amplitude waves and may well reduce the growth rate of those unstable waves.

From Figs. 15b–18b (Fig. 19 shows Fig. 17b in detail) we notice that the integrated value of W_1 is positive in
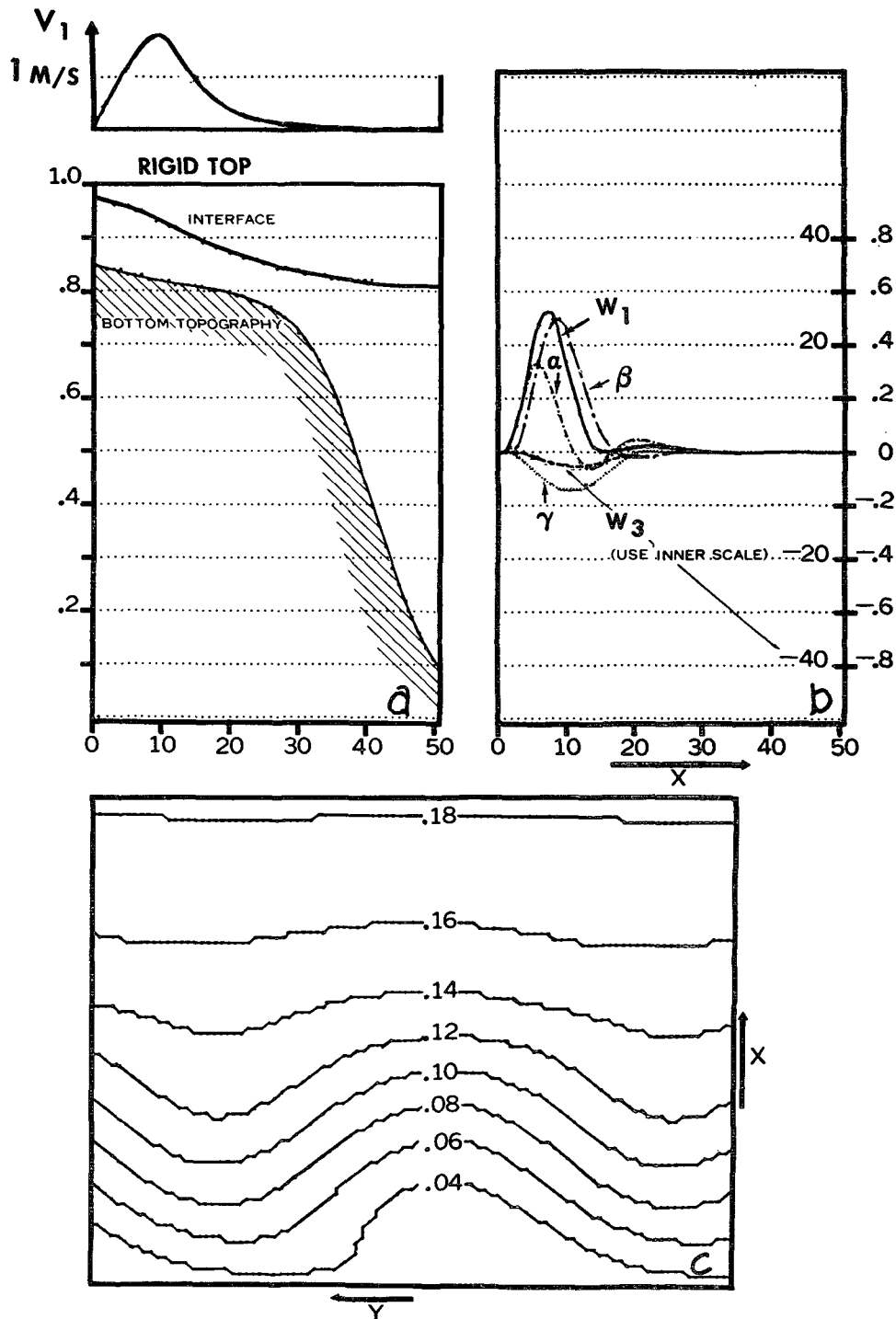
Fig. 17. Same as Fig. 15 except for 33° latitude.

all cases, and the main contributions to it are from the terms $\bar{V}_{1x}\langle U_1 V_1 \rangle \equiv \alpha$ and $\bar{h}_{Ix}\langle U_1 V_1 \rangle \equiv \beta$, where α can be identified as the eddy conversion by Reynolds stress, (for the upper layer) and β as the eddy conversion by Reynolds stress (from both layers); α and β at the left part of the jet show a strong transfer of eddy kinetic energy to the mean flow. This agrees with the observations made by Webster (1961a) in the upper layers in the Gulf Stream south of Cape Hatteras. Curve γ is the transfer of energy due to the vertical Reynolds stress, a transfer of mean kinetic energy to the eddies. The contribution of γ to the integral of W_1 is negative, op-
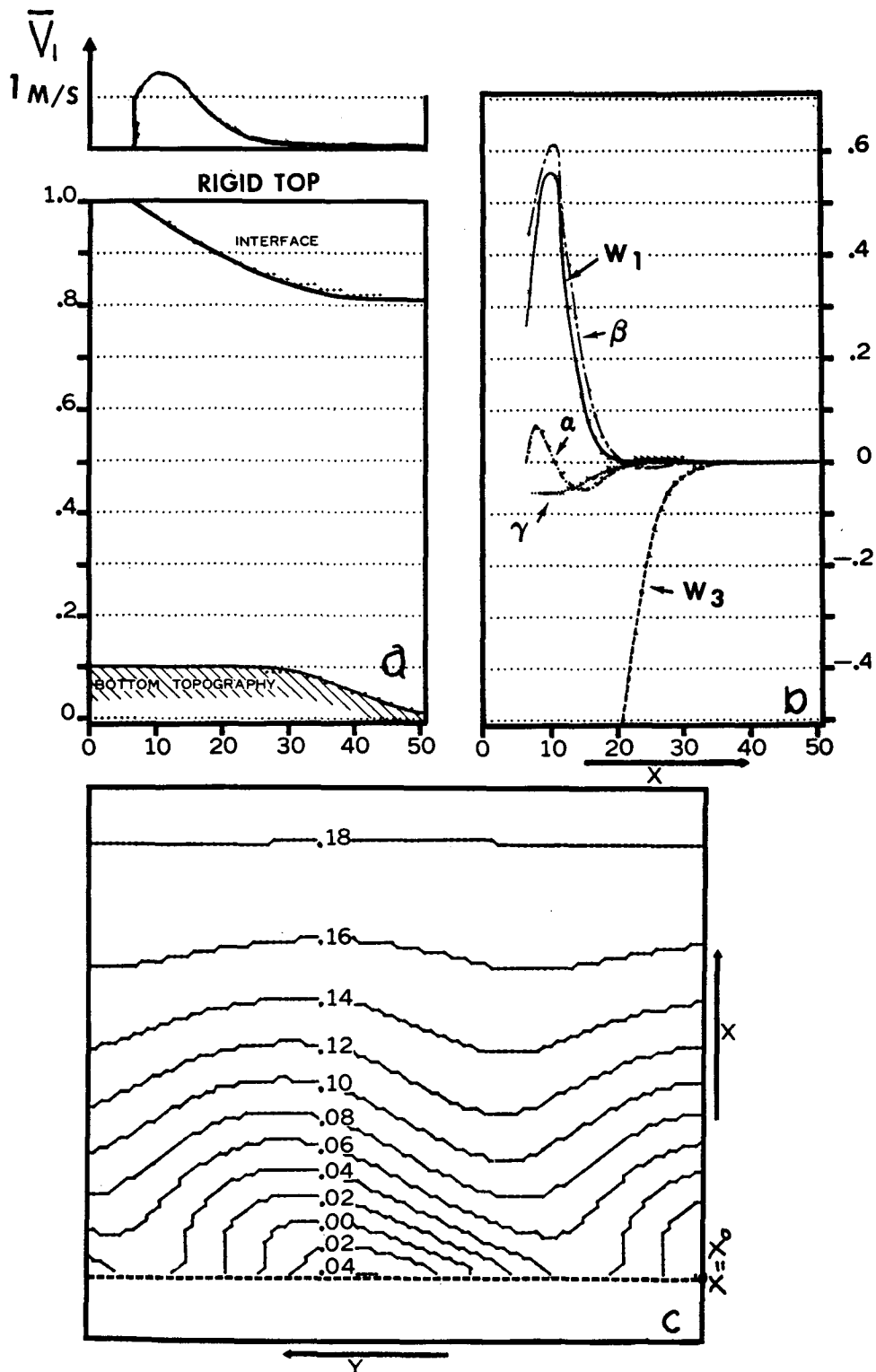
FIG. 18. Same as Fig. 15 except for 37° latitude.

TABLE 1. Baroclinic eigenvalues and parameters of Regions I and II.

Figure	Region	Ro	Ri	μ	$\frac{f}{(10^{-4}}$ $sec^{-1})$	L_s (km)	L_y (km)	V (m sec^{-1})	$\Delta\rho/\bar{\rho}$	$\tau=\tau_r+i\tau_i$	σ_i/f	T (pendulum days)
15	I	0.3	30	1.8	0.7	66.6	226	1.4	1.18×10^{-3}	$-0.13-i0.07$	0.038	6.9
16	I	0.3	20	1.8	0.74	66.6	226	1.48	0.88×10^{-3}	$-0.11-i0.09$	0.049	8.18
17	I	0.3	20	1.8	0.81	66.6	226	1.65	1.09×10^{-3}	$-0.08-i0.086$	0.046	11.62
18	II	0.3*	30	1.8	0.85	150	520	1.45	1.26×10^{-3}	$-0.04-i0.05$	0.014	45.52

* Corresponds to Ro*.

posite in sign to that of α and β, and is small compared with the sum of α and β. The sum of all these terms, W_1, gives the net transfer of kinetic energy from eddies to mean flow. The curve W_3 is the transfer of potential energy from the perturbation to the mean flow. The transfer of potential energy is always negative and much larger than the transfer of kinetic energy (the scale for W_3 is much larger than for W_1 in Figs. 15–18; see Fig. 19) and shows a net transfer from mean energy to the perturbation.

Oort (1964) has made heat flux computations for the same region of the Gulf Stream studied by Webster. Oort's computations indicate a seaward countergradient heat flux across the stream in the surface layer. If baroclinically unstable waves are present, they must release mean potential energy to the eddies. Thus, we would expect that more complete measurements in deeper layers of the Gulf Stream would show a net shoreward heat flux, supplying the necessary potential energy to maintain the baroclinically unstable waves.

To explain why a different transfer in the upper and lower levels is physically reasonable, we consider a two-layer system instead of the continuously stratified flow, keeping in mind the limitation of such a system. It is not difficult to show that if there is a loss of mean potential energy in one of the layers, then there must be a gain of mean potential energy in the other layer. The proof is as follows:

The potential energy of the system is the sum of the potential energy in each layer, i.e.,

$$P_T = P_1 + P_2, \qquad (7.1)$$

where

$$P_2 = \int_{h_B}^{h_I} g\rho_2 z \, dz \quad \text{and} \quad P_1 = \int_{h_I}^{H_T} g\rho_1 z \, dz.$$

Thus,

$$P_T = g\rho_2 \left(\frac{h_I^2 - h_B^2}{2} \right) + g\rho_1 \left(\frac{H_T^2 - h_I^2}{2} \right), \qquad (7.2)$$

and the local time derivative of the mean potential energy is

$$\frac{\partial P_M}{\partial t} = \frac{g\rho_2}{2} \left(\frac{\partial \langle h_I \rangle^2}{\partial t} \right) + \frac{g\rho_1}{2} \left(\frac{\partial - \langle h_I \rangle^2}{\partial t} \right), \qquad (7.3)$$

where the first term on the right-hand side is the time-rate-of-change of mean potential energy of layer 2 and the second term is the time-rate-of-change of the mean potential energy in layer 1. Thus, any change in one of the layers implies a change of the opposite sign in the other layer. In the present study in which baroclinic unstable waves exist, we have $\partial P_M/\partial t < 0$. Since $\rho_2 > \rho_1$ we can conclude from 7.3 that at least for this simple, two-layer system the lower layer is a source of potential energy to the eddies, while the opposite is true in the upper layer.

Figs. 15c–18c show the kinematics of these unstable waves. (As mentioned earlier, these are not the most unstable ones for each region. However, the kinematics
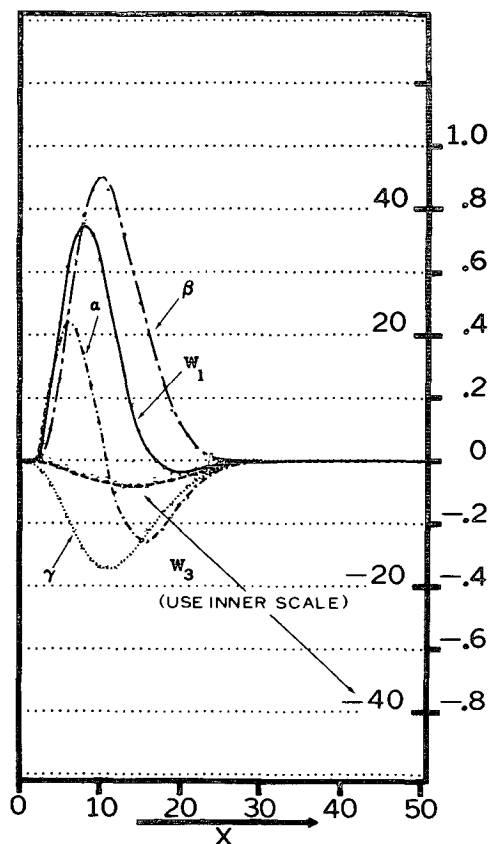

FIG. 19. The relative magnitude of different types of energy transfer (see text).

will be similar.) Most of the figures show some slight asymmetry in the cross-stream gradient of depth on either side of the ridge. A similar asymmetry has been observed in the currents of the Gulf Stream by Webster (1961b). These two results can be related through the geostrophic approximations, and the existence of this phenomenon can be explained in the same way that Starr (1948) has done for atmospheric waves—any kind of motion where the eddies transfer kinetic energy to the mean flow will have this structure, due to the positive correlation of U_1 and V_1 ($\langle U_1 V_1 \rangle > 0$).

As the eddy transfer of kinetic energy intensifies, there will be a tendency to form a shingled structure along the front of the Gulf Stream due to the nonlinear interaction of the finite baroclinic waves with the mean flow. This type of structure has been observed in the Gulf Stream by von Arx et al. (1955).

In view of these results it appears that observational efforts should not be centered on the surface dynamics of the Gulf Stream alone, but should involve the whole vertical structure of the Gulf Stream. Such observations will enable one to compute these energy transfers (e.g., the conversions of mean potential energy to eddy potential energy, and mean kinetic energy to eddy kinetic energy) which are necessary in order to gain a deeper understanding of the behavior of the Gulf Stream.

REFERENCES

Charney, J. G., 1947: The dynamics of long waves in a baroclinic westerly current. *J. Meteor.*, 4, 135–162.

Duxbury, A. C., 1963: An investigation of stable waves along a velocity shear boundary in a two-layer sea with a geostrophic flow regime. *J. Marine Res.*, 21, 246–283.

Eady, E., 1949: Long waves and cyclonic waves. *Tellus*, 1, No. 3, 33–52.

Greenspan, H. P., 1963: A note concerning topography and inertial currents. *J. Marine Res.*, 21, 147–154.

Haurwitz, B., and H. Panofsky, 1950: Stability and meandering of the Gulf Stream. *Trans. Amer. Geophys. Union.*, 31, 723–731.

Lipps, F., 1963: Stability of jets in a divergent barotropic flow. *J. Atmos. Sci.*, 20, 120–129.

Oort, A., 1964: Computation of the eddy heat and density transport across the Gulf Stream. *Tellus*, 14, 55–63.

Orlanski, I., 1968 (FM068): Instability of frontal waves. *J. Atmos. Sci.*, 25, 178–200.

Pedlosky, J., 1964: The stability of currents in the atmosphere and in the ocean. Part I. *J. Atmos. Sci.*, 21, 201–219.

Phillips, N., 1963: Geostrophic motion. *Rev. Geophys.*, 1, 123–176.

Robinson A., and P. Niiler, 1967: The theory of inertial currents. *Tellus*, 19, 269–291.

Starr, V. P., 1948: An essay on the general circulation of the earth's atmosphere. *J. Meteor.*, 5, 39–43.

Stern, M., 1961: The stability of thermo-clinic jets. *Tellus*, 13, 123–125.

Stommel, H., 1953: Examples of the possible role of mature and stratification in the dynamics of the Gulf Stream system. *J. Marine Res.*, 12, 184–195.

von Arx, W. S., 1962: *Introduction to Physical Oceanography.* Reading, Mass., Addison-Wesley, 422 pp.

——, D. Bumpus and W. S. Richardson, 1955: On the fine structure of the Gulf Stream front. *Deep Sea Res.*, 3, 46–65.

Webster, F., 1961a: The effect of meanders on the kinetic energy balance of the Gulf Stream. *Tellus*, 13, 392–401.

——, 1961b: A description of Gulf Stream meanders off Onslow Bay. *Deep Sea Res.*, 8, 130–143.

Warren, B., 1963: Topographical influences on the path of the Gulf Stream. *Tellus*, 15, 2, 167–183.